Cross-Scale Interactions between Electron and Ion Scale Turbulence in a Tokamak Plasma

S. Maeyama* and Y. Idomura
Japan Atomic Energy Agency, 178-4-4 Wakashiba, Kashiwa, Chiba 277-0871, Japan

T.-H. Watanabe
Department of Physics, Nagoya University, Nagoya 464-8602, Japan

M. Nakata, M. Yagi, and N. Miyato
Japan Atomic Energy Agency, 2-166 Obuchi-Omotedate, Rokkasho-mura, Kamikita-gun, Aomori 039-3212, Japan

A. Ishizawa and M. Nunami
National Institute for Fusion Science, 322-6 Oroshi-cho, Toki, Gifu 509-5292, Japan
(Received 29 December 2014; published 23 June 2015)

Multiscale gyrokinetic turbulence simulations with the real ion-to-electron mass ratio and β value are realized for the first time, where the β value is given by the ratio of plasma pressure to magnetic pressure and characterizes electromagnetic effects on microinstabilities. Numerical analysis at both the electron scale and the ion scale is used to reveal the mechanism of their cross-scale interactions. Even with the real-mass scale separation, ion-scale turbulence eliminates electron-scale streamers and dominates heat transport, not only of ions but also of electrons. Suppression of electron-scale turbulence by ion-scale eddies, rather than by long-wavelength zonal flows, is also demonstrated by means of direct measurement of nonlinear mode-to-mode coupling. When the ion-scale modes are stabilized by finite-β effects, the contribution of the electron-scale dynamics to the turbulent transport becomes non-negligible and turns out to enhance ion-scale turbulent transport. Damping of the ion-scale zonal flows by electron-scale turbulence is responsible for the enhancement of ion-scale transport.

DOI: 10.1103/PhysRevLett.114.255002 PACS numbers: 52.65.Tt, 52.30.Gz, 52.35.Ra

Introduction.—Microinstabilities and associated turbulent transport in magnetized plasma are a key issue in magnetic fusion research. In particular, since fusion-born α particles dominantly heat electrons, electron heat transport is critically important for burning plasma experiments. Despite its importance, understanding of electron heat transport is not yet well established because of the difficulty of handling its multiscale nature. Electron heat transport is inherently governed by multiscale plasma turbulence, from extremely fine electron scales at a wavelength on the order of the electron thermal gyroradius ρ_{te} [e.g., the electron temperature gradient modes (ETGs)] to fine ion scales at a wavelength on the order of the ion thermal gyroradius ρ_{ti} [such as the ion temperature gradient modes (ITGs), and the trapped electron modes (TEMs)] [1].

ETG turbulence accompanied by radially elongated eddies (so-called streamers) has long been regarded as a candidate to be the main cause of anomalous electron heat transport [2,3]. Although earlier works typically assume a scale separation between ETG and ITG/TEM turbulence and resolve turbulence at only the electron scales, the possibility of cross-scale interactions has also been explored [4–6]. Theoretical analysis suggests that electron-scale turbulence is sensitive to shearing by relatively short-wavelength ion-scale turbulence, but the reaction in the other direction, from electron scales to ion scales, is supposed to be weak [7]. This notion is also supported by recent gyrokinetic simulation studies such as Refs. [8–10], where the ITG turbulence strongly suppresses the ETG turbulence and dominates heat transport of both ions and electrons. Previous simulations have been limited, using only reduced ion-to-electron mass ratios ($m_i/m_e = 400, 900$) and electrostatic approximation, that is, at the limit of zero plasma pressure ($\beta = 0$). However, the latest comparison with experiments showed that reduced-mass simulation failed to provide even qualitative insight for marginally stable ITG turbulence [11]. The succeeding work also suggested the importance of real-mass multiscale simulation, but the underlying physics is thoroughly left to be revealed [12]. Therefore, the following points remain to be clarified for the more general case: (i) whether the multiscale interactions play a role in reduction of the electron heat transport even with the real hydrogen-to-electron mass ratio ($m_i/m_e = 1836$), where the electron and ion scales are separated by a factor of the square root of the mass ratio when their temperatures are the same; and (ii) whether ion-scale turbulence dominates heat transport even when the real β value is used, which means that electromagnetic (finite-β) effects stabilize the ITGs. To resolve these issues, we carry out multiscale

ITG/TEM/ETG plasma turbulence simulations, employing the real mass ratio and the finite β value, which are first realized by developing a massively parallel algorithm for the finite-difference and spectral methods used in the electromagnetic gyrokinetic simulation code GKV [13–15].

Numerical experiments yield clear answers to the above questions. (i) There are significant cross-scale interactions, even with the real mass ratio. (ii) When the ITGs are stabilized by finite-β effects, contributions from electron scale turbulence are non-negligible. The resultant heat transport in multiscale turbulence deviates from that in single-scale turbulence because of the influence of cross-scale interactions. In contrast to previous studies that have described suppression of electron-scale turbulence by ion-scale turbulence (the $i \to e$ interaction), we newly discovered that electron-scale turbulence can influence ion-scale turbulence via damping of zonal flows and thereby enhance turbulent transport (the $i \leftarrow e$ interaction).

Simulation model.—GKV solves the time evolution of ion and electron distributions and electromagnetic fluctuations in a flux-tube model [14], where compressional magnetic field perturbations are neglected because of $\beta \ll 1$ [16]. Plasma parameter values are set to be the so-called Cyclone DIII-D base case parameters: the density and temperature gradient ratio are set at $L_n/L_{T_i} = L_n/L_{T_e} = 3.1$, the temperature ratio at $T_i/T_e = 1$, the safety factor at $q = 1.4$, the magnetic shear at $\hat{s} = 0.78$, and the inverse aspect ratio at $r/R = 0.18$ [8]. Extending the work of previous studies, we here employ the real hydrogen-to-electron mass ratio and the experimentally relevant β value, letting $m_i/m_e = 1836$ and $\beta \equiv 2\mu_0(n_iT_i + n_eT_e)/B^2 = 2.0\%$, where μ_0 and B denote, respectively, vacuum permeability and magnetic field strength. Both the electron and ion scales are modeled in a simulation box of $-48\rho_{\rm ti} < x < 48\rho_{\rm ti}$, $-47\rho_{\rm ti} < y < 47\rho_{\rm ti}$, $-\pi < z < \pi$, $-4v_{\rm ts} < v_\parallel < 4v_{\rm ts}$, and $0 < \mu < 8T_s/B$ with a resolution of $1024 \times 1024 \times 64 \times 96 \times 16$ grid points. Coordinates represent the radial, poloidal, and parallel space coordinates, the parallel velocity, and the magnetic moment, in that order. As a benchmark, we also carry out a multiscale turbulence simulation at the electrostatic limit ($\beta = 0.04\%$). The required computational costs were ~120 h for the electrostatic case and ~420 h for the electromagnetic case, using 12 288 nodes (98 304 cores) on the K computer, the current flagship supercomputer in Japan [17].

Multiscale instabilities and turbulence.—Linear growth rates of multiscale instabilities are shown in Fig. 1(a), where the effects of the real mass ratio and β value can be clearly identified. Low wave number modes at $k_y\rho_{\rm ti} < 0.6$ are ITGs, and TEMs at $k_y\rho_{\rm ti} \sim 1$ (distinguished from sensitivities to collisionality and mirror force) smoothly connect to high wave number ETGs. The wave numbers providing the maximum growth rate of the ITGs and ETGs

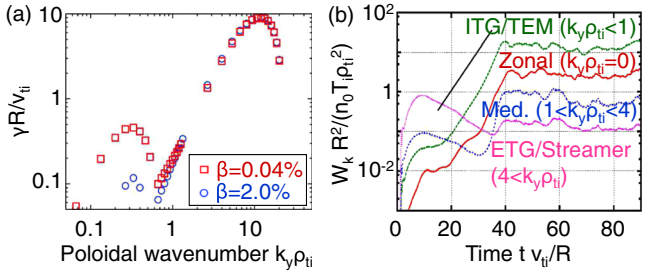

FIG. 1 (color online). (a) Linear instabilities: Linear growth rate γ, plotted against the poloidal wave number k_y. Square (red) and circular (blue) marks indicate electrostatic ($\beta = 0.04\%$) and electromagnetic ($\beta = 2.0\%$) cases, respectively. (b) Nonlinear evolution: Time evolution of the field energy $W_{\boldsymbol{k}}$ for the $\beta = 2.0\%$ case. The solid (red), long-dashed (green), short-dashed (blue), and dotted (rose) lines correspond to the zonal ($k_y\rho_{\rm ti} = 0$), ITG/TEM ($k_y\rho_{\rm ti} \le 1$), intermediate ($1 < k_y\rho_{\rm ti} \le 4$, represented as Med.), and ETG ($4 < k_y\rho_{\rm ti}$) modes, respectively. The straight line shows the slope of the linear growth rate of the ITG with $\gamma = 0.12 v_{\rm ti}/R$.

are $k_y\rho_{\rm ti} \sim 0.3$ and $k_y\rho_{\rm ti} \sim 12$ ($k_y\rho_{\rm te} \sim 0.3$), respectively, which are separated by the square root of the ion-to-electron mass ratio, $\sqrt{m_i/m_e} \sim 43$. Comparison of the two cases with different β values shows that ITGs are stabilized by the finite-β effects [18], while the ETGs are unaffected by β. Microtearing modes and kinetic ballooning modes, which are also candidates for anomalous electron and ion heat transport in high-β plasma [19,20], are not destabilized in the tested cases.

The time evolution of multiscale turbulence calculated with the real mass ratio and β value is presented in Fig. 1(b). The field energy of a Fourier mode is denoted by $W_{\boldsymbol{k}} = \langle [\varepsilon_0 k_\perp^2 + \sum_s e_s^2 n_0/T_s(1-\Gamma_{0s\boldsymbol{k}})]|\phi_{\boldsymbol{k}}|^2/2 + k_\perp^2|A_{\parallel\boldsymbol{k}}|^2/(2\mu_0)\rangle$, where ε_0, $\Gamma_{0s\boldsymbol{k}}$, $\phi_{\boldsymbol{k}}$, and $A_{\parallel\boldsymbol{k}}$ are the vacuum permittivity, a gyrophase average operator in the wave number $\boldsymbol{k}$ space, the electrostatic potential, and the parallel component of the vector potential, respectively. Small-scale ETGs rapidly grow, and their growth is saturated by creating radially elongated streamers, where extremely fine ($4 < k_y\rho_{\rm ti}$) modes account for more than 80% of the field energy. Although ETG turbulence dominates before $tv_{\rm ti}/R = 20$, the ITGs grow linearly, suppressing the ETG turbulence in the interval $20 < tv_{\rm ti}/R < 40$. As a result, even with the real mass ratio and β value, ITG turbulence with zonal flows (characterized by $k_y = 0$ modes) becomes dominant in the quasisteady state found in the later phase of the simulation.

The resultant heat transport spectra are shown in Fig. 2. As a reference, we also plot the spectra of single-scale "low-k" and "high-k" simulations, resolving only ion scales ($k_y\rho_{\rm ti} < 1.3$) or electron scales ($k_y\rho_{\rm ti} > 1.3$), respectively, where the parameter values are the same as used for the multiscale "full-k" simulation (except the perpendicular box sizes or resolutions). In the electrostatic case ($\beta = 0.04\%$), where the ITGs are highly unstable, the

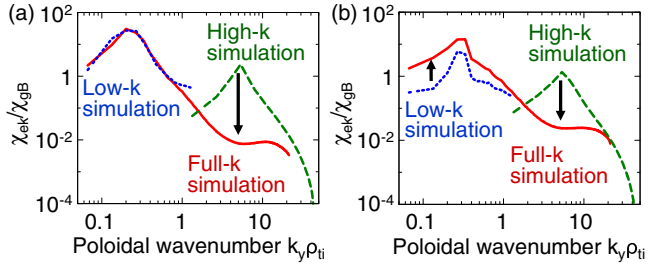

FIG. 2 (color online). Poloidal wave number spectrum of the time-averaged electron energy diffusivity χ_{ek} for (a) electrostatic ($\beta = 0.04\%$) and (b) electromagnetic ($\beta = 2.0\%$) cases. The solid (red), dotted (blue), and dashed (green) lines plot χ_{ek} as obtained from the full-k, low-k ($k_y\rho_{ti} < 1.3$), and high-k ($k_y\rho_{ti} > 1.3$) simulations, respectively.

ion-scale turbulence strongly suppresses the electron-scale modes and dominates the energy diffusivity of both ions and electrons. In that case, the low-k simulation shows reasonable agreement with the full-k case [Fig. 2(a)]. In the electromagnetic case ($\beta = 2.0\%$), where the linear growth rates of ITGs are reduced by finite-β effects, it is additionally seen that the ion-scale turbulence dominates energy diffusivity. Compared with the electrostatic case, however, the suppression of the electron-scale transport is relatively weak, and the remaining electron-scale turbulence leads to enhancement of the ion-scale transport, the level of which is threefold that in the low-k simulation [Fig. 2(b)]. This means that the electron-scale turbulence can influence the ion-scale dynamics when the ion-scale instabilities are weak. Because of these cross-scale interactions, the transport spectrum in multiscale turbulence is not a simple sum of single-scale spectra. We note that the ion energy diffusivity exhibits similar behavior. The total ion energy diffusivity in the electrostatic case ($\beta = 0.04\%$) is $\chi_i = 19.3\chi_{gB}$, and the electron energy diffusivity is $\chi_e = 6.3\chi_{gB}$ in the gyro-Bohm units $\chi_{gB} = v_{ti}\rho_{ti}^2/R$; these results are consistent with the values given in the literature [8,10]. In the electromagnetic case ($\beta = 2.0\%$), although the ion energy diffusivity is reduced to $\chi_i = 3.6\chi_{gB}$, the electron energy diffusivity maintains a level similar to before, at $\chi_e = 4.4\chi_{gB}$. This is because the transport caused by the magnetic flutter compensates for the reduction of transport caused by $\boldsymbol{E}\times\boldsymbol{B}$ convection.

Cross-scale interactions.—The multiscale gyrokinetic turbulence simulations clearly demonstrate that there are cross-scale interactions between electron and ion scale turbulence, even when using the real mass ratio, and that ITG turbulence can be dominant even when growth rates are reduced by the finite-β effects. To clarify the cross-scale interactions, we analyze the gyrokinetic entropy transfer [21], written as

$$I_{\boldsymbol{k}} = \sum_{\boldsymbol{p}}\sum_{\boldsymbol{q}} J_{\boldsymbol{k}}^{\boldsymbol{p},\boldsymbol{q}}, \tag{1}$$

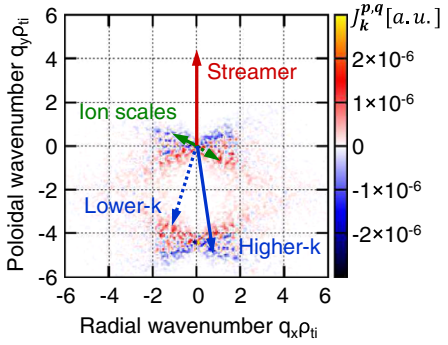

FIG. 3 (color online). Wave number $\boldsymbol{q}$ spectrum of the triad transfer $J_{\boldsymbol{k}}^{\boldsymbol{p},\boldsymbol{q}}$ (normalized by $n_0T_iv_{ti}\rho_{ti}^2/R^3$) for a typical streamer $\boldsymbol{k} = (0, 4.4\rho_{ti})$, averaged over $60 < tv_{ti}/R < 80$ with $\beta = 2.0\%$. Arrows represent dominant triad couplings. Negative and positive values of $J_{\boldsymbol{k}}^{\boldsymbol{p},\boldsymbol{q}}$, respectively, mean that the streamer gives and receives entropy via coupling with resonant modes $\boldsymbol{k}+\boldsymbol{p}+\boldsymbol{q} = 0$.

where the triad transfer is given by

$$J_{\boldsymbol{k}}^{\boldsymbol{p},\boldsymbol{q}} = \sum_s \delta_{\boldsymbol{k}+\boldsymbol{p}+\boldsymbol{q},\boldsymbol{0}} \frac{\boldsymbol{b}\cdot\boldsymbol{p}\times\boldsymbol{q}}{2B} \times \mathrm{Re}\left[\left\langle \int dv^3 (\bar{\psi}_{s\boldsymbol{p}} g_{s\boldsymbol{q}} - \bar{\psi}_{s\boldsymbol{q}} g_{s\boldsymbol{p}}) \frac{T_s g_{s\boldsymbol{k}}}{F_{sM}} \right\rangle\right], \tag{2}$$

with the gyrophase-averaged generalized potential at $\bar{\psi}_{s\boldsymbol{k}} = (\bar{\phi}_{\boldsymbol{k}} - v_\parallel \bar{A}_{\parallel\boldsymbol{k}})$ and the nonadiabatic part of the perturbed distribution function at $g_{s\boldsymbol{k}}$ for the species s. Angle brackets $\langle\cdots\rangle$ denote the flux-surface average. The gyrokinetic entropy transfer is regarded as a kinetic generalization of the fluid Reynolds and Maxwell stresses, and describes the driving or damping of the mode via nonlinear mode coupling, that is, via the $\boldsymbol{E}\times\boldsymbol{B}$ and magnetic nonlinearities. Under the resonant condition $\boldsymbol{k}+\boldsymbol{p}+\boldsymbol{q} = \boldsymbol{0}$, the triad transfer satisfies the symmetry condition $J_{s\boldsymbol{k}}^{\boldsymbol{p},\boldsymbol{q}} = J_{s\boldsymbol{k}}^{\boldsymbol{q},\boldsymbol{p}}$ and the detailed balance $J_{s\boldsymbol{k}}^{\boldsymbol{p},\boldsymbol{q}} + J_{s\boldsymbol{q}}^{\boldsymbol{k},\boldsymbol{p}} + J_{s\boldsymbol{p}}^{\boldsymbol{q},\boldsymbol{k}} = 0$. The exact gyrokinetic form is employed for evaluating the net transfer in Fig. 4(a), but we use a fluid approximation of the triad transfer based on the Hermite and Laguerre expansion (for $v_\parallel$ and μ, respectively) up to the third-order moments in Fig. 3. This reduces the computational cost for the analysis while still maintaining sufficient accuracy.

We now apply triad transfer analysis to investigate the suppression of the electron-scale transport by the ion-scale turbulence. Figure 3 shows that the nonlinear entropy transfer of electron-scale streamers is dominated by short-wavelength ($k_\perp\rho_{ti} \sim 1$) ITG turbulent eddies, rather than by long-wavelength zonal flows or electron-scale modes. Via nonlinear mode coupling with short-wavelength ITG turbulent eddies, the normal entropy cascade occurs, meaning that the streamer receives entropy from lower wave number ($k_\perp\rho_{ti} < 4.4$) modes and passes it

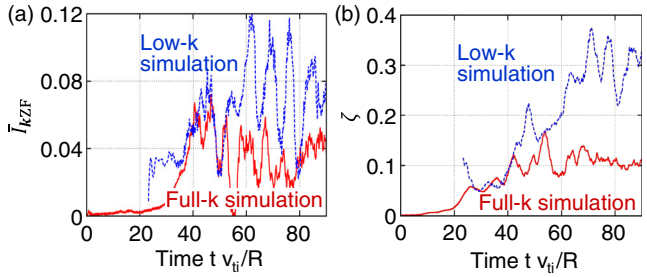

FIG. 4 (color online). (a) Ratio of zonal-mode entropy transfer to the total entropy drive $\bar{I}_{\boldsymbol{k}\mathrm{ZF}} = \sum_{k_y=0} I_{\boldsymbol{k}}/X_{\mathrm{drive}}$ and (b) ratio of zonal to nonzonal field energy $\zeta = \sum_{k_y=0} W_{\boldsymbol{k}}/\sum_{k_y\neq 0} W_{\boldsymbol{k}}$ (where $\beta = 2.0\%$). The solid (red) and dashed (blue) lines indicate results from the full-k and low-k ($k_y\rho_{\mathrm{ti}} < 1.3$) simulations, respectively.

to higher wave number ($k_\perp\rho_{\mathrm{ti}} > 4.4$) modes. These direct measurements of nonlinear mode-to-mode interactions provide explicit evidence for one of Holland's suggestions: electron-scale turbulence may be sensitive to shearing by relatively short-wavelength ion-scale turbulence [7].

Additionally, we investigate the mechanism of the enhancement of ion-scale transport by electron-scale turbulence in the $\beta = 2.0\%$ case. Although one possible mechanism for enhancement is direct driving of ITG turbulence via an inverse cascade from electron-scale turbulence, electron-scale turbulence is governed by the normal cascade, as shown by triad transfer analysis (Fig. 3). The ITG turbulence seems to be saturated through the coupling with zonal flows, as is often observed in studies of ITGs. Hence, by focusing on zonal flows, we compare the results of the full-k simulation with those of the low-k one, which starts from $t = 23R/v_{\mathrm{ti}}$ (i.e., at the beginning of the ITG linear growth). In Fig. 4(a), the entropy transfer from turbulent (nonzonal) modes to zonal modes is plotted as $\bar{I}_{\boldsymbol{k}\mathrm{ZF}} = \sum_{k_y=0} I_{\boldsymbol{k}}/X_{\mathrm{drive}}$, normalized by the driving term in the entropy balance equation, $X_{\mathrm{drive}} = \sum_s (T_s\Gamma_s/L_{p_s} + \Theta_s/L_{T_s})$, where Γ_s and Θ_s are the turbulent particle and heat fluxes, respectively, and $L_{p_s}^{-1} = L_n^{-1} + L_{T_s}^{-1}$ [22]. This demonstrates that the full-k simulation generates zonal modes less efficiently than the low-k simulation, which excludes the electron-scale dynamics. In other words, electron-scale turbulence weakens the generation of zonal flows. More specifically, a detailed triad transfer analysis shows that the zonal modes are generated by mainly ion-scale turbulence, and electron-scale turbulence contributes to damping of the zonal modes, which reduces the generation rate by ~20%. The zonal-mode damping effect is clearly found in the time evolution of the ratio of zonal to nonzonal field energy $\zeta = \sum_{k_y=0} W_{\boldsymbol{k}}/\sum_{k_y\neq 0} W_{\boldsymbol{k}}$, plotted in Fig. 4(b). The ratio of zonal to nonzonal field energy in the full-k simulation is lower than that in the low-k simulation. The absolute value of the field energy and the shearing rate of the zonal flows are comparable between the two simulations. This indicates that ITG instability growth is saturated when sufficiently strong zonal flows are generated. Because the zonal flow generation rate in the full-k simulation is smaller than that in the low-k simulation, ion-scale turbulence in the full-k simulation has to be enhanced more strongly, so that it keeps the zonal flows strong enough via the Reynolds stress. As a result, ion-scale turbulence in the full-k simulation is driven at a higher level than that in the low-k simulation. Although we note that saturation processes of turbulence are not only limited to zonal flow generation (but also inverse energy cascade, etc.,), zonal flows and their damping may play important roles near the marginal stability condition such as the Dimits shift [23]. Indeed, in the $\beta = 2.0\%$ case, the ITGs are close to marginal stability due to electromagnetic stabilization, and the electron-scale turbulence exerts a damping effect on the ion-scale zonal flows and leads to transport enhancement, which is not observed in the single-scale low-k simulation. This damping effect also occurs in the electrostatic case ($\beta = 0.04\%$), but its contribution there is negligible relative to ion-scale turbulence when the ITGs are strongly unstable. Finally, we refer to a study employing experimental inputs and geometry, which showed that electrostatic multiscale simulations would also give enhanced low-k transport in the case of weak ITG instability [12]. Their results support the importance of cross-scale interactions in real experiments, and can be explained by the mechanisms presented here.

Summary.—This study examined multiscale ITG/TEM/ETG turbulence, revealing that cross-scale interactions exist, even when the real mass ratio and a finite β value are used. Ion-scale turbulence is found to strongly suppress electron-scale turbulence and dominate heat transport of both ions and electrons. When the ITGs are less unstable as a consequence of finite-β effects, the damping effect of electron-scale turbulence on ion-scale zonal modes is considerable and enhances the transport levels. These results suggest that simulations resolving only the ion-scale dynamics give good estimates when the ion-scale modes are highly unstable. However, when the ion-scale modes are near marginal stability, the influence of electron-scale turbulence is an important factor in characterizing the turbulent transport of ions and electrons, acting through effective damping of ion-scale zonal flows. These new findings urge us to innovate our view of turbulent transport from a conventional scale separation approach to a multi-scale paradigm, and provide a valuable insight into the physics of multiscale turbulence on two different energy injection scales.

This work was supported by the HPCI Strategic Program Field No. 4, the JAEA-NIFS collaboration program, and the MEXT KAKENHI Grant No. 26800283. Computations were performed on the K computer at the RIKEN Advanced Institute for Computational Science through

the HPCI System Research project (Project ID: hp120011), and on Helios at the Computational Simulation Centre of the International Fusion Energy Research Centre (IFERC-CSC).

*smaeyama@p.phys.nagoya-u.ac.jp
Present address: Department of Physics, Nagoya University, Nagoya 464-8602, Japan.

[1] W. Horton, Rev. Mod. Phys. **71**, 735 (1999).
[2] W. Dorland, F. Jenko, M. Kotschenreuther, and B. N. Rogers, Phys. Rev. Lett. **85**, 5579 (2000).
[3] F. Jenko, W. Dorland, M. Kotschenreuther, and B. N. Rogers, Phys. Plasmas **7**, 1904 (2000).
[4] S. I. Itoh and K. Itoh, Plasma Phys. Controlled Fusion **43**, 1055 (2001).
[5] J. Li and Y. Kishimoto, Phys. Rev. Lett. **89**, 115002 (2002).
[6] F. Jenko, J. Plasma Fusion Res. Ser. **6**, 11 (2004).
[7] C. Holland and P. H. Diamond, Phys. Plasmas **11**, 1043 (2004).
[8] J. Candy, R. E. Waltz, M. R. Fahey, and C. Holland, Plasma Phys. Controlled Fusion **49**, 1209 (2007).
[9] R. E. Waltz, J. Candy, and M. R. Fahey, Phys. Plasmas **14**, 056116 (2007).
[10] T. Görler and F. Jenko, Phys. Rev. Lett. **100**, 185002 (2008).
[11] N. T. Howard, A. E. White, M. Greenwald, C. Holland, and J. Candy, Phys. Plasmas **21**, 032308 (2014).
[12] N. T. Howard, C. Holland, A. E. White, M. Greenwald, and J. Candy, Phys. Plasmas **21**, 112510 (2014).
[13] T.-H. Watanabe and H. Sugama, Nucl. Fusion **46**, 24 (2006).
[14] S. Maeyama, A. Ishizawa, T.-H. Watanabe, N. Nakajima, S. Tsuji-Iio, and H. Tsutsui, Comput. Phys. Commun. **184**, 2462 (2013).
[15] S. Maeyama, T.-H. Watanabe, Y. Idomura, M. Nakata, M. Nunami, and A. Ishizawa, Plasma Fusion Res. **8**, 1403150 (2013).
[16] N. Joiner, A. Hirose, and W. Dorland, Phys. Plasmas **17**, 072104 (2010).
[17] S. Maeyama, T.-H. Watanabe, Y. Idomura, M. Nakata, M. Nunami, and A. Ishizawa, Parallel Comput. (to be published).
[18] J. Y. Kim, W. Horton, and J. Q. Dong, Phys. Fluids B **5**, 4030 (1993).
[19] H. Doerk, F. Jenko, M. J. Pueschel, and D. R. Hatch, Phys. Rev. Lett. **106**, 155003 (2011).
[20] S. Maeyama, A. Ishizawa, T.-H. Watanabe, M. Nakata, N. Miyato, M. Yagi, and Y. Idomura, Phys. Plasmas **21**, 052301 (2014).
[21] M. Nakata, T.-H. Watanabe, and H. Sugama, Phys. Plasmas **19**, 022303 (2012).
[22] H. Sugama, T.-H. Watanabe, and M. Nunami, Phys. Plasmas **16**, 112503 (2009).
[23] M. Nakata and Y. Idomura, Nucl. Fusion **53**, 113039 (2013).